

Journal Pre-proofs

Development of an innovative flexible paper-based methanol fuel cell (PB-DMFC) sensing platform – application to sarcosine detection

Liliana P. T. Carneiro, Alexandra M. F. R. Pinto, M. Goreti F. Sales

PII: S1385-8947(22)05042-2
DOI: <https://doi.org/10.1016/j.cej.2022.139563>
Reference: CEJ 139563

To appear in: *Chemical Engineering Journal*

Received Date: 31 July 2022
Revised Date: 18 September 2022
Accepted Date: 30 September 2022

Please cite this article as: L. P. T. Carneiro, A. M. F. R. Pinto, M. Goreti F. Sales, Development of an innovative flexible paper-based methanol fuel cell (PB-DMFC) sensing platform – application to sarcosine detection, *Chemical Engineering Journal* (2022), doi: <https://doi.org/10.1016/j.cej.2022.139563>

This is a PDF file of an article that has undergone enhancements after acceptance, such as the addition of a cover page and metadata, and formatting for readability, but it is not yet the definitive version of record. This version will undergo additional copyediting, typesetting and review before it is published in its final form, but we are providing this version to give early visibility of the article. Please note that, during the production process, errors may be discovered which could affect the content, and all legal disclaimers that apply to the journal pertain.

© 2022 Published by Elsevier B.V.



1 **Development of an innovative flexible paper-based methanol fuel cell**
2 **(PB-DMFC) sensing platform – application to sarcosine detection**

3 *Liliana P. T. Carneiro^{*1,2,3,4}, Alexandra M. F. R. Pinto⁴, M. Goreti F. Sales^{**1,2}*

4 ¹BioMark@UC, Department of Chemical Engineering, Faculty of Sciences and Technology, Coimbra
5 University, Portugal

6 ²BioMark@ISEP, School of Engineering, Polytechnic Institute of Porto, Portugal

7 ³CEB, Centre of Biological Engineering, Minho University, Portugal

8 ⁴CEFT, Department of Chemical Engineering, Faculty of Engineering, University of Porto, Portugal

9
10
11
12
13
14
15
16
17
18 ** To whom the correspondence should be addressed. BioMark, Sensor Research@UC, Department of
19 Chemical Engineering, Faculty of Sciences and Technology of Coimbra University, Rua Sílvio Lima,
20 Polo II, 3030-790 Coimbra, Portugal. Tel.: +351239798733; E-mail: goreti.sales@gmail.com;
21 goreti.sales@eq.uc.pt
22

23 **Abstract**

24 This work describes for the first time a paper-based direct methanol fuel cell platform (PB-DMFC) that functions
25 as an energy source and biosensor, assembled on a simple paper substrate for point-of-care (POC) applications,
26 targeting sarcosine as proof-of-concept.

27 Specifically, a methanol fuel cell strip was developed from a square of Whatman paper, acting as substrate. The
28 paper strip was treated with an impermeable agent (paraffin solution) and supported all fuel cell device components,
29 including the electrolyte (Nafion[®]), anode electrode (carbon black Pt/Ru), cathode electrode (carbon black Pt), and
30 current collectors (silver edges). All the described components formed a flexible single layer that operated in a
31 completely passive mode by adding few microliters of a methanol solution on the anode side and by using
32 atmospheric oxygen on the cathode side. The obtained platform had a stable electrical signal with an average OCV
33 value of 0.45-0.55V and a maximum power density of 20-50 μ W/cm², depending on the methanol concentration
34 used (0.5M – 2M). A sensing layer was built in situ on the anode electrode by electropolymerization of a solution
35 of 3,4-ethylenedioxythiophene (EDOT) and pyrrole (Py) as monomers. The obtained PB-DMFC/biosensor was
36 calibrated at room temperature in buffer and healthy human urine and showed linear responses from 1.0×10^{-7} to
37 1.0×10^{-3} M with a detection limit of 6.6×10^{-8} M. Selectivity studies evidenced signals changing within 1-10%, both
38 in positive and negative directions. Results evidenced good reproducibility.

39 Overall, the obtained results demonstrate a self-sufficient biosensor for the detection of sarcosine consisting of an
40 innovative paper-based methanol fuel cell strip. This concept can open new horizons for massification of biosensors
41 even in places with energy shortage.

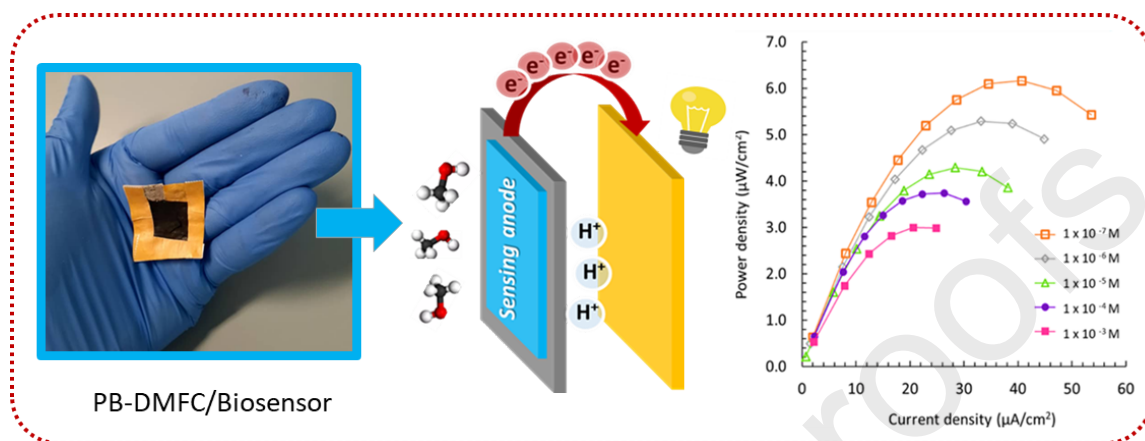
42

43

44 *Keywords:* Paper-based methanol fuel cell; sensing platform; molecularly imprinted polymer; sarcosine; point of
45 care; cancer biomarker.

46 Graphical abstract

47



48

49

50 1. Introduction

51 Paper-based analytical devices appear to be a promising technology to produce simple, low-cost,
52 lightweight, disposable, and portable devices that have greater potential for point-of-care (POC)
53 applications [1,2]. Paper is considered a promising and ideal substrate for the development of analytical
54 devices because it is inexpensive, available, environmentally friendly, biocompatible, flexible, and easily
55 modified [3,4]. Compared to plastics and synthetic polymers, the biodegradability of paper substrates
56 makes them promising environmentally friendly biomaterials for use in flexible electronic applications,
57 combined with the ability to tailor treatments to desired properties [5,6]. Since Whitesides and colleagues
58 [7] combined paper-based devices with microfluidic technology, a large number of new multifunctional
59 devices with different architectures and detection modes can be found in the literature [8–11]. The
60 combination with electrochemical detection is of particular interest as it allows faster response with higher
61 sensitivity and selectivity [12].

62 An ideal paper-based electrochemical analyzer should have all functions built directly into the
63 integrated instrument, including independence from the power source, so that it can be easily operated
64 outside the laboratory [13]. To obtain self-powered paper-based analytical platforms, paper-based
65 microfluidic fuel cells have shown promise for diagnostic and sensing applications [14,15]. These types
66 of devices consist of cellulose paper as the support of the electrode/membrane system and are based on
67 the laminar flow of anolyte and catholyte side by side, powered by different types of fuels. Several
68 examples of these types of systems have been described in the literature, including microfluidic fuel cells
69 driven by an ethanol-dichromate fuel-oxidant mixture [16], hydrogen fuel cells [17,18], methanol-KOH
70 fuel cells [19] and formic acid fuel cells [20,21]. All of these systems appear to be capable of powering
71 small devices for short periods of time. However, in most cases, their architecture is not simple and
72 additional components such as valves, mixers, separators, and pumps are required. In addition, the analysis

73 of samples and the incubation process are poorly understood in terms of the design of the platform relative
74 to the energy generated.

75 In the work presented here, this drawback has been overcome by developing a paper-based methanol
76 fuel cell platform that functions simultaneously as power source and biosensor, all combined in a simple
77 square paper layer. A strip was developed to build a direct methanol fuel cell using a commercial Whatman
78 paper as the substrate (PB-DMFC) that supports all the fuel cell components, such as the electrolyte
79 membrane (Nafion[®]), carbon anode and cathode electrodes, and current collector. No additional
80 components are needed; the system works with only 100 μL of an aqueous methanol solution added
81 directly to the anode side of the paper device. Since the device is primarily made of paper, it is completely
82 flexible and represents an innovative, flexible paper-based fuel cell platform. Apart from some similarity
83 to microfluidic fuel cells, the system presented here cannot be considered a microfluidic fuel cell as it
84 operates on a completely different approach, which is more like conventional passive methanol fuel cells
85 (DMFCs). Passive DMFCs appear to be a promising power generation technology that can be applied in
86 the field of portable power [22,23], and the simple setup we have developed may open up new
87 opportunities to bring biosensors from the laboratory to the field.

88 Integration of the biosensor function was achieved by developing a biosensor film of molecularly
89 imprinted polymer (MIP) directly on the anode of the paper device. This sensor film was prepared by
90 electropolymerization of charged poly(3,4-ethylenedioxythiophene) (PEDOT) and polypyrrole (PPy)
91 monomers in situ, in the presence of sarcosine, which was selected as the target molecule here. The
92 electropolymerization approach used here makes it possible to obtain a sensing polymeric layer with
93 cavities tailored to sarcosine, capable of affecting the power generated by PB-DMFC in a concentration-
94 dependent manner. When the rebinding of sarcosine occurs, the access of methanol to the platinum catalyst
95 nanoparticles is hindered and consequently the performance of the device decreases, transforming the

96 paper-based fuel cell into a biosensor sensitive to the detection of sarcosine. It is important to highlight
97 that this fuel cell paper strip allows direct incubation of the sample in the sensing area, indicating that this
98 fuel cell setup is suitable as a user-friendly sensing platform. In addition, simple and user-friendly self-
99 powered sensor platforms can also be used in resource-limited areas to promote the worldwide diffusion
100 of biosensors.

101 To the best of the authors' knowledge, this is the first work to report on a flexible, single-layer,
102 paper-based methanol fuel cell platform that serves simultaneously as an energy source and biosensor and
103 can actually be used as a wearable device. The selection of sarcosine as a target is related to the increasing
104 importance of this biomolecule in the diagnosis and progression of prostate cancer [24]. Sarcosine is an
105 *N*-methyl derivative of the amino acid glycine that has been identified in prostate cancer tumor tissue [25]
106 and can also be found in the urine of men, highlighting the importance of this new urinary biomarker for
107 diagnostic/prognostic testing in prostate cancer [26,27]. Sarcosine levels have been reported to increase
108 with progression of prostate cancer [28], from the normal concentration value of 0.60 μM to over 2.67 μM
109 which is a strong indication of prostate cancer [29].

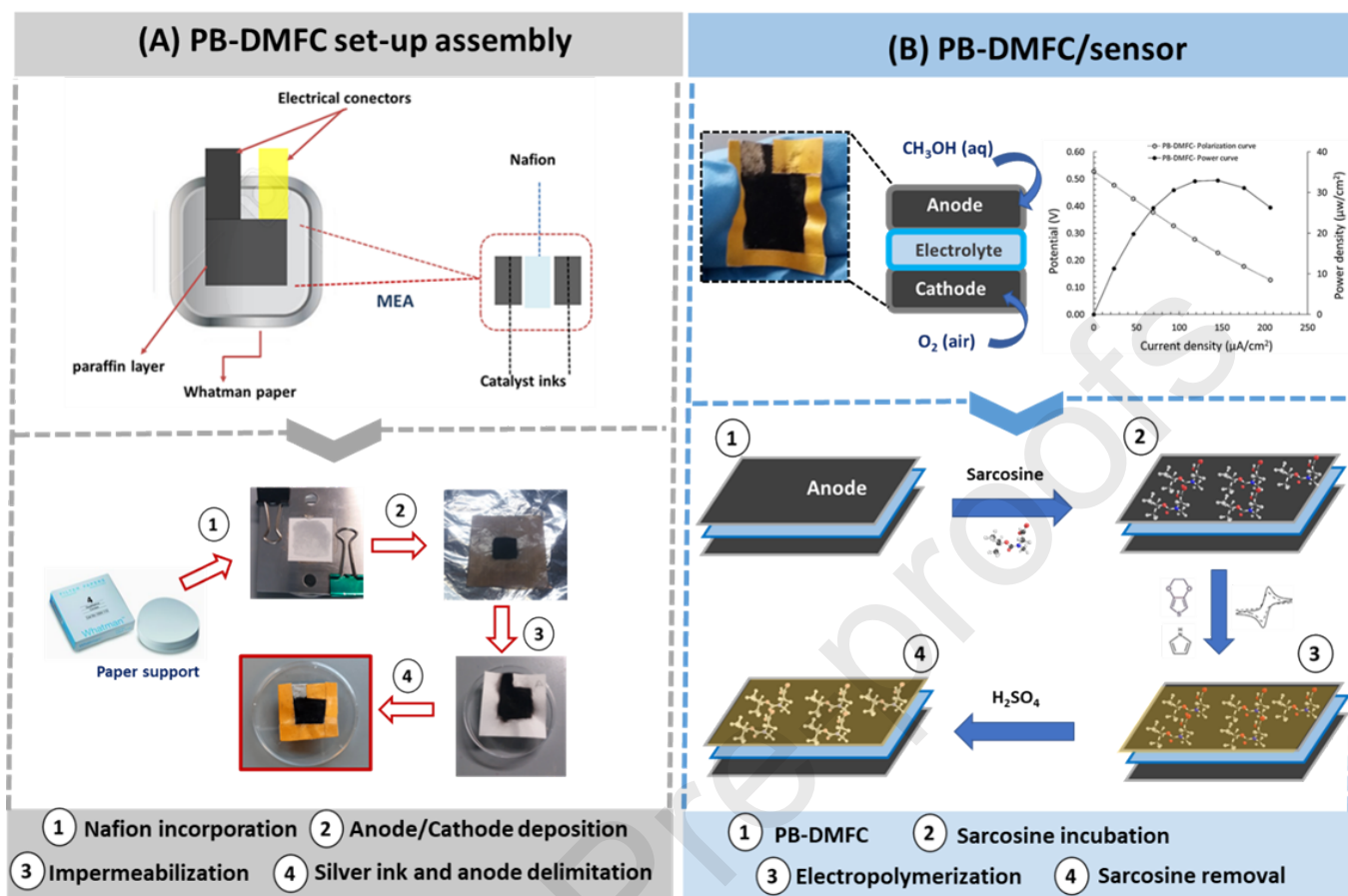
110 Thus, a simple paper-based methanol fuel cell (bio)sensor platform was developed, to be feed with
111 few microliters of an aqueous methanol solution and atmospheric oxygen, without auxiliary components.
112 The sensing element layer is developed on the anode side of the fuel cell strip, which is fabricated by an
113 electropolymerization process of EDOT/pyrrole monomers. The final sensor platform was tested against
114 sarcosine under buffered conditions and in real human urine sample. In addition, selectivity studies were
115 performed with various interfering factors to verify the reliability of the developed sensor platform.

116

117 **2. Experimental section**

118 *2.1 Paper based Fuel Cell assembly*

119 The PB-DMFC involves several steps, including electrolyte deposition, anode/cathode electrode
120 deposition, impermeability stabilisation, and current collector deposition. The different steps involved in
121 this setup have been schematically shown in [Figure 1A](#) and supplemented with real images. All
122 components form a single layer consisting of a commercial Whatman strip paper impregnated with 200
123 μL of a Nafion[®] solution (20 wt% in alcohols, 100 μL per side of the paper), which acts as a solid protonic
124 electrolyte allowing the protons transport and preventing electrons conduction (electron insulator). A
125 square metal mould with an area greater than 2.25 cm^2 was used to ensure complete distribution of the
126 electrolyte. The mould was heated at room temperature for 20 minutes and then at 60 °C for 10 minutes
127 to dry the polymer (not completely). The resulting composite material acts as a proton exchange membrane
128 (PEM), replacing the solid Nafion[®] film used in typical methanol fuel cell devices. The impregnated paper
129 was glued to another mould with the desired active area of 2.25 cm^2 and placed on a hot plate at 60 °C.
130 Using an airbrush pen, the composite membrane was coated on both sides with two different carbon inks
131 prepared in propanol, which also contained 20% Nafion[®] as a binder. For the anode side, an ink containing
132 carbon black with Pt/Ru (40:20 wt%) was used, and for the cathode side, an ink containing carbon black
133 with Pt (10 wt%) was used. The catalyst inks were stirred overnight to obtain a homogeneous solution and
134 to avoid clogging of the airbrush. The Pt/Ru alloy in the anode and the Pt nanoparticles in the cathode are
135 the best catalysts for the oxidation of methanol and the reduction of oxygen in the respective electrodes
136 used in methanol fuel cells [30].



137

138 **Figure 1.** Schematic representation of the various steps required to obtain an (A) PB-DMFC assembly on
 139 the paper substrates, which includes: the incorporation of the electrolyte, the deposition of the
 140 anode/cathode inks, the paraffin impermeabilization and the silver ink current collectors. after the
 141 fabrication of the PB-DMFC platform and the evaluation of the electrochemical reaction (B) a sarcosine-
 142 sensitive MIP layer was obtained by electropolymerization on the anode side using EDOT/PPy monomers,
 143 and later the sarcosine template is removed under acidic conditions.

144

145 A solution of diluted paraffin in propanol (50/50) was added surrounding the active area of the PB-
 146 DMFC, at 90 °C, in order to waterproof the paper and avoid the paper breakdown. On top of the anode
 147 surface, a thin layer of a diluted solution of paraffin (~10 %) was added to slightly hydrophobized the
 148 surface, in order to hinder the MeOH crossover from the anode to the cathode side.

149 Later, the system was electrically connected with a silver conductive ink on the upper edges of the
150 device (one connecting the anode and the other the cathode) in different paths. The setup was left at 60 °C
151 for 10 minutes to cure the silver ink. To complete the paper device, tape was placed on the back of each
152 electrical connection to prevent short circuits, and it was also placed around the entire anode side to
153 delineate the active area.

154 The PB-DMFC works with aqueous methanol solutions with concentrations between 0.5 and 2 M
155 (adsorbed in adsorbent paper) and with atmospheric O₂. The adsorbent square paper covers the entire
156 anode surface and distributes the methanol solution homogeneously over the entire surface of the electrode
157 (which also prevents methanol leakage). During the electrochemical measurements, a square glass (FTO)
158 was used to cover the anode side of the PB-DMFC unit to prevent the methanol from evaporating. The
159 fuel cell device can also be operated without the cover glass and without the adsorbent paper, but with
160 these two components the system reaches stability in a shorter time, so that several consecutive
161 measurements can be performed without changing the methanol solution.

162

163 *2.2. Biosensor element preparation*

164 The Pt nanoparticles in the anode are the material directly related to the sensing capability, because
165 the obstruction of the Pt nanoparticles by sarcosine molecules affects the methanol oxidation rate, which
166 is key to the sensing capability of the fuel cell. To incorporate this sensing capability, a suitable
167 PEDOT/pyrrole semiconductor polymer was developed on the anode in the presence of sarcosine, which
168 allows specific sites to be obtained in the polymer after the release of sarcosine by acid electrochemical
169 treatment. The incorporation of the sensing element into the system PB-DMFC (Figure 1B) was achieved
170 by an electropolymerization process (in a 3-electrode system) of a solution of EDOT (0.01 M) and pyrrole
171 (0.005 M) in PBS buffer (previously flushed with N₂) directly on the anode side of the fuel cell unit. First,

172 a solution of sarcosine (1.0×10^{-3} M) was incubated in the anode for $t = 2$ h. Then, the PB-DMFC was
173 carefully washed with ultrapure water and dried with nitrogen and incorporated into the 3-electrode
174 system; in this configuration the anode layer of the PB-DMFC is the working electrode, a leakage-free
175 Ag/AgCl plastic electrode is the reference electrode, and a platinum rod electrode is the counter electrode.
176 Electropolymerization was performed by cyclic voltammetry (CV) (10 cycles, -0.3 V to 1.2 V) at a scan
177 rate of 25 mV/s. The same CV protocol was used to remove the sarcosine template, but a 0.5 M H_2SO_4
178 solution was used instead of the monomer solution.

179 In parallel, the non-imprinted fuel cells (PB-DMFC / NIP) were prepared using exactly the same steps and
180 protocols, except for the incubation of the sarcosine template. The polymer layer was a barrier to the
181 spread of methanol on the anode surface. Therefore, special care was taken to ensure that the polymer was
182 semipermeable enough to allow the methanol molecules to reach the catalytic Pt nanoparticles and
183 maintain the electrochemical activity (hence, in the unprinted PB-DMFCs, the electrochemical signal is
184 attenuated by the presence of the polymer film). The polymer-modified PB-DMFCs (printed and
185 unprinted) were not reusable and were discarded after calibration.

186

187 **3. Results and discussion**

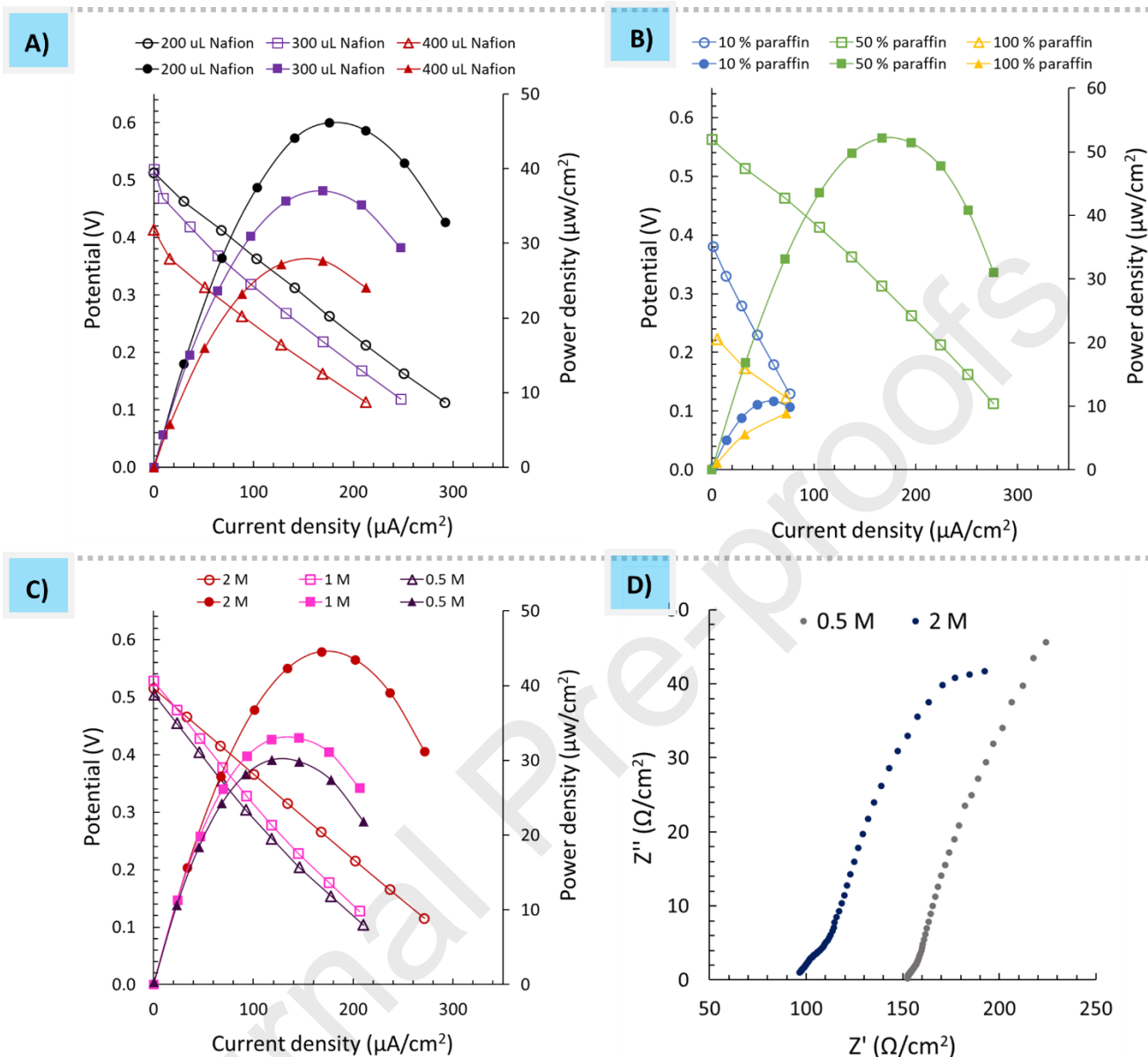
188

189 *3.1 Assembly of the Paper based fuel cell device*

190 *3.1.1. Configuration*

191 The design of the paper-based fuel cell includes all components necessary for operation, which are built
192 into the paper strip. Several prototypes were tested to find a suitable design that would provide a simple
193 and durable configuration with a stable electrical signal. [Figure S1](#) shows and describes all the prototypes
194 that were studied during the work, as well as the changes that were made to each setup until the final

195 prototype presented here, PB-DMFC, was found. Additional studies were performed on the selected
196 prototype to improve the measured OCV and output power. The ideal amount of Nafion[®] electrolyte
197 impregnated into the paper and the amount of paraffin solution to efficiently hydrophobize the fuel cell
198 system were evaluated in terms of the overall performance of the PB-DMFCs by tracking the polarization
199 and power curves for all assembled systems. [Figure 2A-B](#) shows the obtained results normalized to the
200 active area (2.25 cm²) of the assemblies recorded with 2M MeOH. The ideal amount of Nafion[®] electrolyte
201 incorporated into the paper was studied and the results are shown in [Figure 2A](#). As one can see, using a
202 small amount of Nafion[®] solution (200 μ L) gives better results in terms of power/current density and OCV
203 of the different PB-DMFCs assemblies tested. The use of larger amounts of Nafion[®] electrolyte makes it
204 difficult to produce a homogeneous layer, resulting in some roughness on the surface of the electrolyte
205 dry film. This roughness, achieved with larger amounts of Nafion[®], can affect the proton conductivity of
206 the system, resulting in lower performance, which is more evident in the 400 μ L impregnated PB-DMFC.
207 Considering these results, the selected volume of Nafion[®] electrolyte was set at 200 μ L, which is the
208 minimum volume required to cover the entire active area of the paper substrate.



209

210 **Figure 2.** Electrochemical data of PB-DMFCs in terms of polarization (empty symbols) and power curves
 211 (full symbols) obtained under different test conditions: **(A)** the Nafion[®] electrolyte incorporated into the
 212 paper matrix; **(B)** the paraffin amount used as an impermeabilizing agent; **(C)** operation of the device
 213 using various methanol concentrations in the range of 0.5-2.0 M; and **(D)** electrochemical impedance
 214 spectroscopy measurements under open-circuit conditions (OCV) using 0.5 and 2.0 M methanol
 215 concentrations.

216

217 The paraffin-impermeabilizing agent was first tested without dilution (100%) and later diluted in
218 isopropanol (10% and 50%), as shown in [Figure 2B](#). The results obtained show a significant difference
219 when the paraffin amount was varied from 10% to 100%, with the ideal value being in the middle (50%).
220 These results are easily understood considering the important and crucial role of the paraffin component.
221 With only 10% of this compound, the transfer of methanol from the anode to the cathode cannot be
222 avoided, resulting in a lower OCV value and lower power. The poisoning of the cathode electrode by
223 methanol molecules is a problem of DMFCs that lowers their performance and makes their conversion
224 difficult so far [28,29]. In a system of this type, composed mainly of paper, it is even more difficult to
225 limit the methanol crossover, but a compromise was found with a solution of 50% paraffin and a stable
226 system with a fairly acceptable OCV (≈ 0.55 V) and a reasonable performance was obtained. Paraffin
227 works very well in preventing methanol crossover, but it has an insulating behaviour (no conductive link)
228 that was observed when a pure paraffin solution was spread in the PB-DMFC array. When undiluted
229 paraffin is used, the conductivity of the system is severely compromised, resulting in the lower measured
230 OCV (0.22 V) and power output. Based on these results, the selected amount of impermeabilizing agent
231 was set at 50% (paraffin/IPA) and adopted in the work. It is important to emphasize that this paraffin/IPA
232 ratio refers to the vicinity of the active anode/cathode region. A light layer of 10% (paraffin/IPA) was
233 applied to the anode side of the PB-DMFC to limit the transfer of methanol.

234

235 *3.1.2. Selection of ideal MeOH concentration*

236 Passive direct methanol fuel cells are usually operated with concentrated MeOH solutions (between
237 1 and 5 M) [31]. A compromise between the ideal MeOH concentration in the anode layer and the rate of
238 MeOH transfer from the anode to the cathode layer is essential to maximize cell voltage and reduce power
239 losses. This compromise strongly depends on the fuel cell structure and design [32]. Thus, in this PB-

240 DMFC setup, the generated power is mainly limited by the simplest arrangement, and the use of higher
241 methanol concentrations can lead to higher methanol crossover, which affects the performance of PB-
242 DMFCs, especially the useful life, since the methanol crossover poisons the Pt nanoparticle catalysts on
243 the cathode side. In addition, the interface between the fuel and the Nafion[®] paper-based electrolyte is
244 very narrow in this developed setup, so the ideal methanol concentration to achieve a stable electrical
245 signal in successive measurements was investigated. Various methanol concentrations were tested,
246 ranging from 2.0 to 0.5 M. The corresponding polarization and power curves are shown in [Figure 2-C](#).
247 These results were obtained using the same PB-DMFC starting with the higher MeOH concentration to
248 the lowest MeOH concentration, washing with ultrapure water, and drying with N₂ after stabilization at
249 each concentration. The results show that both the power density and current density increase with
250 increasing MeOH concentration, and the MeOH concentration varies more in the range of [2.0-1.0 M]; in
251 the range of [1.0-0.5 M], the difference in power density and current density is very small. Therefore, after
252 successive measurements (washing and changing the MeOH fuel), the electrical signal is more stable
253 when using 0.5 M MeOH than when using the 2 M concentration (results obtained with different PB-
254 DMFCs), with relative standard deviations ranging from 2% to 4% for the lowest concentration, while the
255 relative standard deviations range from 10% to 14% for the 2.0 M MeOH concentration (data in [Figure](#)
256 [S2](#)). Therefore, when using the less concentrated MeOH solution (0.5 M), the loss in performance is
257 compensated by the gain in long-term stability of the PB-DMFC platforms, as the MeOH crossover is
258 significantly reduced (fewer MeOH molecules involved in the reaction also means fewer MeOH
259 molecules passing through the Nafion[®]/paper membrane to the cathode side).

260 Electrochemical impedance spectroscopy (EIS) measurements were also performed to record the
261 resistance of the PB-DMFCs under open circuit voltage (OCV) in two different methanol concentrations.
262 The obtained results are shown in [Figure 2-D](#), normalized to the active area of the PB-DMFC assembly

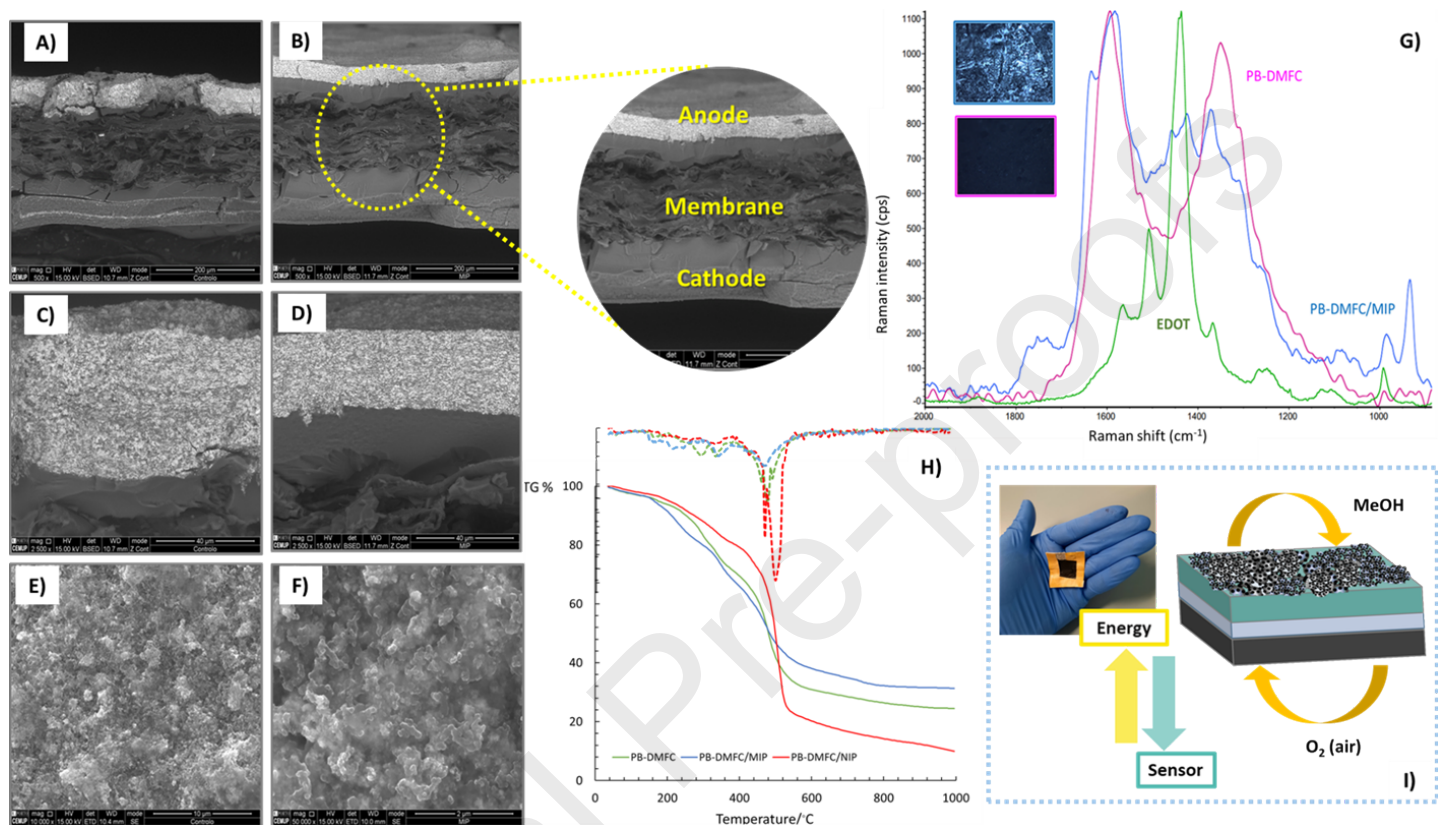
263 (2.25 cm²). The EIS data was also fit to obtain the equivalent circuits of each individual fuel cell set-up
264 (Figure S4), to estimate the ohmic resistance (R_{ohm}), activation resistance (R_{act}) and mass transfer (R_{mt})
265 of the whole fuel cell. The measured resistance values are quite high compared to a complex typical DMFC
266 array consisting of all components [33]. However, higher values have been observed in simpler arrays
267 with micro-DMFC systems because the simplicity of the system conditions the various mass transport
268 phenomena [34,35]. This measured electrical resistance is related to the electrical resistances of the two
269 anode/cathode electrodes, the proton transfer of the membrane, the current collector pathways and also
270 the resistances between the individual components. Since the PB-DMFC contains all the components in a
271 simple paper square without hot pressing and additional components, these resistance values in the order
272 of 100-150 Ω/cm^2 are quite acceptable for a first simple prototype. When the highly concentrated 2.0 M
273 MeOH solution is used, a lower resistance is measured compared to the dilute 0.5 M MeOH concentration.
274 Therefore, the difference in measured resistance using the two different MeOH concentrations is not
275 significant and considering that this platform needs to be activated and calibrated in a process with several
276 consecutive measurements, higher signal stability is very important, so the lowest methanol concentration
277 of 0.5 M is selected for further studies.

278

279 *3.2. PB-DMFC device characterization*

280 The PB-DMFC assemblies (unmodified and modified with polymer sensing material) were analysed with
281 a scanning electron microscope (SEM) to evaluate the distribution of the different assembled layers
282 (anode, electrolyte, and cathode) and to obtain evidence of the anchored polymer layer in the anode-side
283 surface. The SEM diagrams of a PB-DMFC and a PB-DMFC/MIP in cross-section and surface topography
284 are shown in Figure 3A-F.

285



286

287

288 **Figure 3.** Characterization results of the paper fuel cells developed in this work: SEM Cross-sectional images of a (A) control cell PB-
 289 DMFC and a (B) polymer modified PB-DMFC /MIP; (C) overview of the anode layer of PB-DMFC and (D) PB-DMFC /MIP showing
 290 differences in the structure of the catalytic layer; topography analysis of (E) PB-DMFC and (F) PB-DMFC /MIP showing different
 291 roughness. Raman analysis at 532 nm for a control sample PB-DMFC, PB-DMFC /MIP and a sample with EDOT carbon support for
 292 comparison; confocal images of a PB-DMFC and PB-DMFC /MIP assemblies highlighting the color difference (blue) (G). TGA and
 293 DTG curves of different paper fuel cell units (PB-DMFC, PB-DMFC /MIP, PB-DMFC / NIP) in an inert atmosphere (nitrogen, 20 mL
 294 min⁻¹, heating rate 30 °C/min) (H). Overview of a PB-DMFC strip showing the chemical reactions responsible for the dual function
 295 (power and sensor) of the developed platform (I)

296 Analysing the cross-sectional images of PB-DMFC (Figure 3A) and PB-DMFC /MIP (Figure 3B), a clear
297 difference in the 3-layer anode/electrolyte/cathode distribution can be seen: In PB-DMFC without
298 modification, the layers were not so well defined because they were easily damaged by breaking with
299 liquid nitrogen. In the polymer modified PB-DMFC/MIP, the 3 layers were very well defined, indicating
300 that some kind of reinforcement protected the layers during fracture with liquid nitrogen. The same results
301 were obtained in the PB-DMFC/NIP samples (Figure S3A-C), indicating the presence of a modification
302 consisting of a homogeneous polymer layer in both the MIP and NIP assemblies. In addition, a higher,
303 well-defined thickness of the anode layer can be seen, indicating the presence of the EDOT-PPy polymer
304 (Figure 3C-D). When analysing the surface topography of the PB-DMFC samples (Figure 3E-F), a
305 differentiated roughness is observed in the PB-DMFC/MIP sample compared to the unmodified PB-
306 DMFC. These results could indicate the presence of a uniform polymer layer anchored on the surface of
307 the PB-DMFC/MIP sample.

308 Both fuel cell configurations showed similar assignments in terms of nanocatalysts (Pt and Ru) and
309 fluorine (from Nafion[®], which was used as a binder). However, an increase in the sulphur element was
310 observed, which could be another indication of the anchoring of PEDOT in the carbon surface (Figure S3-
311 D-E). It is important to highlight that the amount of Pt and Ru catalysts was similar in both samples,
312 indicating that the anode electrode was structurally damaged by the electrochemical
313 polymerization/removal cycles applied to fabricate the PB-DMFC/biosensor.

314 The PB-DMFC and the PB-DMFC/MIP assemblies are also tracked using the Raman technique
315 (Figure 3G). The spectra obtained for the anode side of the unmodified PB-DMFC show the two broad G-
316 bands (1592 cm^{-1}) and D-bands (1344 cm^{-1}) typical of carbon black nanostructures, usually around 1585
317 cm^{-1} and 1350 cm^{-1} [36]. Significant differences are observed when comparing with the spectra obtained
318 for PB-DMFC/MIP, which can be attributed to the polymer anchor in the electropolymerization protocol.

319 The results show a significant distortion of the D-band (1346 cm^{-1}) and the overlapping of some
320 characteristic peaks of the PEDOT polymer (green line, polymer obtained by electropolymerization under
321 the same conditions as the sensors anchored on a square of commercial carbon for comparison). The
322 overlapping peaks of PEDOT appear in the PB-DMFC/MIP spectra at 992 cm^{-1} , 1117 cm^{-1} , and 1433
323 cm^{-1} . Moreover, when analysing the confocal images, one can also observe the difference in the surface
324 colour of PB-DMFC and PB-DMFC /MIP (see [Figure 3G](#)). This shows that the polymer-modified sample
325 has a stronger blue hue, which is characteristic of PEDOT-based polymers [37]. The relative intensity of
326 the D and G bands can be an indicator of the disorder present in a sample, and the ratio I_D/I_G can be
327 calculated to evaluate the defects present in a particular carbon material [38]. The I_D/I_G ratios for the PB-
328 DMFC and the PB-DMFC/MIP sensor were calculated and the final values are the average of 3
329 independent measurements at different points on the anode surface ([Table S1](#)). The PB-DMFC (control)
330 has an I_D/I_G ratio of 0.91, while the sensor PB-DMFC/MIP sensor has a ratio of 0.68. This ratio difference
331 is significant and supports the presence of a uniform polymer layer anchored to the anode surface PB-
332 DMFC.

333 The TGA thermograms and DTG curves of PB-DMFC and polymer modified PB-DMFC/MIP-NIP
334 fuel cells are shown in [Figure 3-H](#). When analysing the corresponding weight loss curves, a differential
335 thermal decomposition behaviour of the different analysed samples can be observed, with PB-DMFC/NIP
336 showing the sharpest mass loss profile. This result is to be expected since PB-DMFC/NIP is the sample
337 with a more homogeneous upper polymer layer, which also has a "protective effect" that causes a shift in
338 the temperature range of decomposition and delays the thermal decomposition of this sample. Thus, the
339 cavities presented in PB-DMFC/MIP do not cause significant differences in the decomposition profile
340 compared to the control (PB-DMFC) because the polymer layer is not as homogeneous due to the presence
341 of the sarcosine template during electropolymerization. All samples can be considered thermally stable,

342 with minimal percent weight loss occurring up to 200°C, including the Nafion[®] layer (membrane adsorbed
343 in the paper separating the anode and cathode sides) and the paraffin hydrophobic agent. The results of
344 comparing a PB-DMFC, a Nafion[®] impregnated paper and a paraffin impregnated paper are shown in
345 [Figure S5](#) and demonstrate the stability and thermal decomposition of these materials in isolated form.

346 Moreover, the described PB-DMFC platforms are stable for several weeks and can be stored at room
347 temperature in a dark and dry environment until use. They can be reused several times without degrading
348 performance if stored under proper conditions. These properties are completely novel for a system of this
349 type and combined with the very simple structure of this assembly (a square of paper) makes this system
350 very promising for use as a portable biosensor that can be used in any location.

351 In summary, the characterization results of this innovative methanol fuel cell yield a stable, durable,
352 and robust system that can be modified with a sensory polymer, transforming this simple, low-cost paper
353 platform into a self-powered system that serves as both an energy source and a sensor ([Figure 3-I](#)). Thus,
354 this platform is user-friendly and easy to transport, which is an important requirement for a point-of-care
355 application.

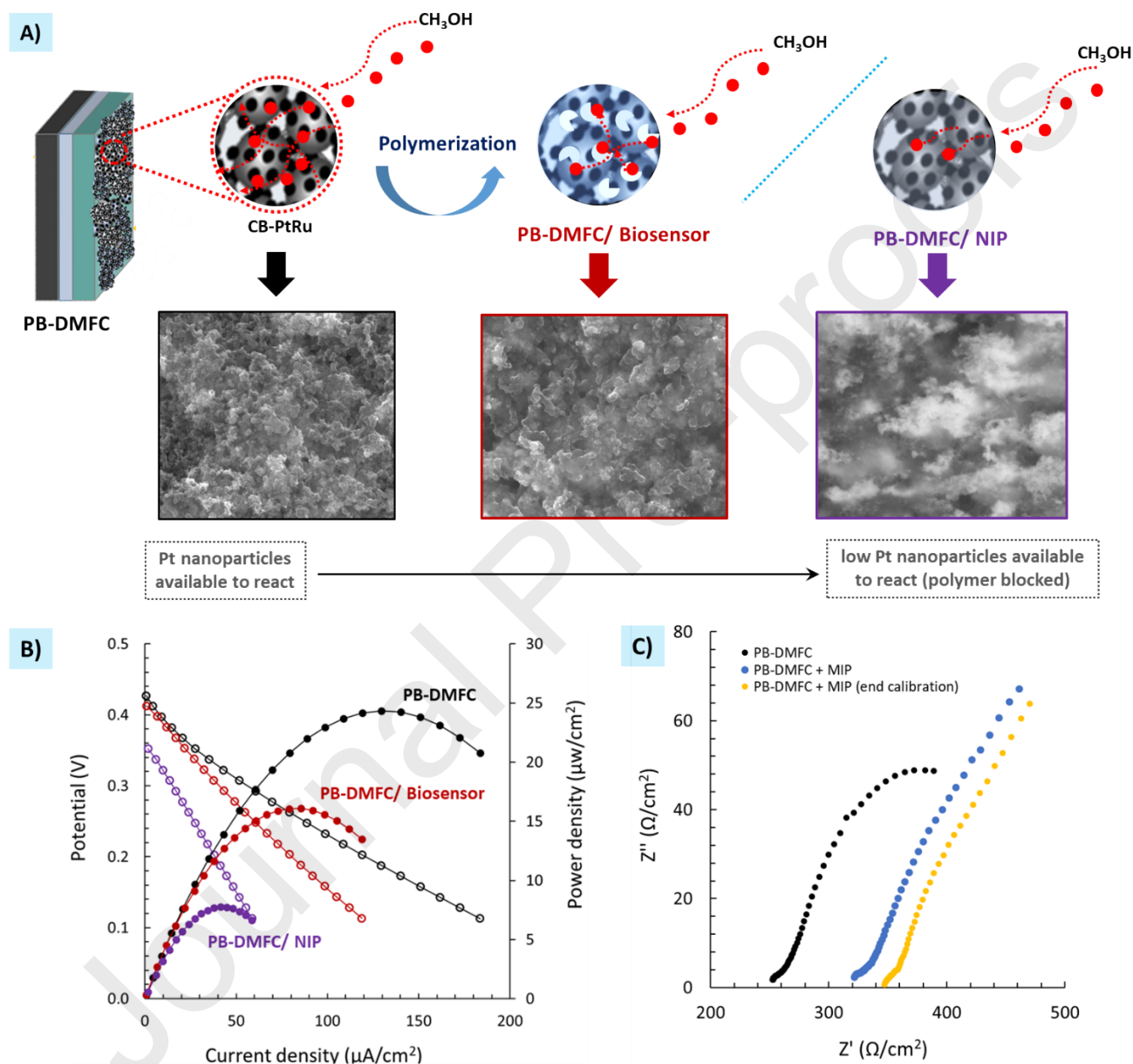
356

357 [3.3 Integration of the sensing area on the PB-DMFC](#)

358 [3.3.1. Imprinted film layer development](#)

359 The sensor layer was built on the surface of the anode layer of the PB-DMFC, creating the PB-
360 DMFC/biosensor. The combination of the imprinted polymers with the anode carbon catalysts makes it
361 possible to obtain a hybrid nanocomposite electrode with a dual function: methanol catalytic activity and
362 sensing property. In fact, this dual function is closely related, since both steps involve the oxidation of
363 methanol in the Pt catalyst sites: in the PB-DMFC the Pt active sites are fully available to react with the
364 methanol molecules, while in the PB-DMFC/biosensor the Pt catalyst sites are less accessible (polymer

365 film) and can be hindered by the incubation of the template or even in a control experiment (non-imprinted
 366 polymers, NIP) the Pt active sites are partially blocked by the polymer layer (Figure 4-A). The SEM
 367 images also show the modifications in the surface of the different anode electrodes.



368
 369 **Figure 4.** Analysis of the behavior of the different fuel cell platforms with respect to (A) general scheme
 370 complemented with surface SEM images evidencing the possible different methanol pathways in the fuel
 371 cell anode electrode and showing the blocking effect of the catalytic Pt active sites in the polymer modified
 372 fuel cells (PB-DMFC/Biosensor and PB-DMFC/NIP). The CB-PtRu is covered by a sarcosine imprinted
 373 film in the PB-DMFC/Biosensor, shown in blue color, or a control film without printed sites in the PB-

374 DMFC/NIP, shown in gray color. The voids in the anode of the PB-DMFC/Biosensor allow a faster and
375 more efficient reaction of the methanol fuel on the surface of the Pt catalysts compared to the polymer
376 layer of the control (without voids), which acts as a barrier for the reaction of the methanol molecules.
377 Comparison of the measured polarization and power curves recorded for the different paper fuel cell
378 systems (PB-DMFC, PB-DMFC/Biosensor, PB-DMFC/NIP) **(B)** and evaluation of the EIS analysis of a
379 PB-DMFC before, after polymerization and at the end of a calibration **(C)**.

380

381 The sensory area in PB-DMFCs was obtained in situ by electropolymerization using cyclic
382 voltammetry (10 cycles in PBS buffer) of EDOT and Py monomers. This electropolymerization approach
383 was investigated and validated in a previously published work [39] in the context of (bio)sensory methanol
384 fuel cells. In this work, a carbon fabric containing PtRu nanoparticles (C/PtRu) was directly modified by
385 the electropolymerization of EDOT/Py and later assembled in a typical passive methanol fuel cell
386 configuration, which showed good electrical properties and sensitive responses to CEA detection.

387 The PB-DMFCs developed in this work are very simple systems compared to the conventional passive
388 fuel cell units used in previous works [39,40]. The advantages of this innovative PB-DMFC strip
389 compared to previous fuel cells developed with a passive configuration [39,40] are based on the simplicity
390 of this new single-layer configuration. The single-layer PB-DMFC allows easy insertion and removal of
391 the methanol fuel and sample for analysis, the volume required for the fuel was very small (100 μL)
392 compared to the volume required to operate the first setup (1500 μL), and no special tools or screws were
393 required to open and close the device. The disadvantage of this simpler fuel cell setup is its low power
394 density compared to the fully passive system developed previously. The lower power density of the PB-
395 DMFC system is compensated by its higher sensitivity and user-friendly approach (since the sensor can
396 only be used once, a higher power output was not a requirement for it to work well). This new design is
397 also less expensive and more environmentally friendly, considering all the materials needed to build the
398 system.

399 The good conducting and electrocatalytic properties of the PEDOT/PPy polymer are important to improve
400 the stability of the PBDMFC/biosensor compared to the unmodified PB-DMFC. The hydrophobic nature
401 of the PEDOT/PPy polymers also contributes to the signal stabilization of the paper-based systems by
402 acting as a barrier to methanol penetration through the anode surface (methanol crossover) and also
403 reduces the electrical blockage caused by the small amount of paraffin added to hydrophobized the anode
404 surface. Therefore, these types of conductive materials have been widely explored to improve the
405 performance and durability of fuel cell systems, which makes them suitable for fuel cell electrode
406 applications [41]. Among the common conductive polymers, PEDOT polymer is particularly attractive
407 and suitable for use in fuel cell electrodes because it is stable and exhibits high electronic conductivity
408 (between 1-100 S/cm, depending on whether a dopant has been added) [42].

409 To obtain a higher density of sites impregnated with sarcosine on the anode surface, the surface was
410 incubated ($t = 2$ h) before polymerization. Removal of sarcosine from the polymeric network was achieved
411 electrochemically in a sulfuric acid solution. This procedure allows the adsorbed sarcosine molecules to
412 be removed and the imprinted cavities to be emptied for subsequent rebinding. In addition to releasing the
413 imprinted molecules from the polymeric network, this removal step in acid also allows the removal of
414 unreacted monomers from the surface and of the paraffin added for the previous activation of the fuel cells
415 (paraffin solution is not acid resistant). Interestingly, the sensor layer obtained in situ is sufficient to
416 control the methanol crossover, resulting in a faster and more durable PB-DMFC system where the right
417 polymer layer takes over the role of paraffin and the sensing property (in the case of PB-DMFC/MIP).

418 An example of a cyclic voltammogram (last $n^{\circ}10$ cycle) in a 3-electrode configuration of the PB-
419 DMFC/biosensor and control PB-DMFC (NIP) are shown in [Figure S6](#), as are the corresponding removal
420 steps. These voltammograms were referenced to a pair of PB-DMFCs that were fabricated on the same
421 day and had similar performances. Exceptional care was taken in the selection of the PB-DMFCs to ensure

422 that they had similar electrical characteristics, despite the "handmade" process involving the various steps
423 in the fabrication of the PB-DMFCs. The analysis of the obtained voltammograms shows that the presence
424 of sarcosine in the PEDOT/PPy electropolymerization leads to a decrease in the electrical resistivity values
425 over the whole applied voltage range. The presence of sarcosine seems to hinder the polymer formation
426 in the anode surface PB-DMFC and its removal allows a significant increase in the electric current, while
427 for the non-printed PB-DMFC /NIP the effect of removal is in the opposite direction; this decrease in PB-
428 DMFC/NIP current could be due to over-oxidation of the PEDOT polymer layer in acidic media causing
429 a decrease in the electrical conductivity [43,44]. Overall, the PB-DMFC/NIP samples allow us to evaluate
430 the influence of the polymer layer on the PB-DMFC performance and also the nonspecific behaviour in
431 sarcosine target binding.

432

433 3.3.2. Impact of the imprinted film in the PB-DMFC

434 The effect of modifying the anode side of the PB-DMFCs with the EDOT/PPy polymer was evaluated by
435 recording and comparing the experimental polarization curves (sampled DC voltammetry technique) until
436 the electrochemical system reached stable maximum potential (OCV) and power. Different paper fuel cell
437 units with similar initial values (before modification) were used for the studies. The obtained results are
438 shown in [Figure 4B](#). Analysis of the polarization curves (blank points) and power curves (filled points) of
439 the two PB-DMFC units indicates that adding the EDOT/PPy polymer on the anode side causes the
440 measured maximum OCV and generated current/power to decrease more significantly for the control (PB-
441 DMFC/NIP). These results were expected since the polymer layer has a blocking effect on the Pt catalyst
442 nanoparticles, which is more pronounced for the sample without voids (PB-DMFC/NIP) than for the PB-
443 DMFC/Biosensor, which is in the middle range in terms of current and power. In terms of maximum
444 power, the initial PB-DMFCs produce 22-25 $\mu\text{A}/\text{cm}^2$ until the PB-DMFC/biosensor produces 16 $\mu\text{A}/\text{cm}^2$

445 and the control PB-DMFC/NIP produces only $8 \mu\text{A}/\text{cm}^2$ after stabilization (successive polarization curves
446 were followed for all systems until the signal deviation is less than 1%). Therefore, the effect of
447 PEDOT/PPy is more pronounced for PB-DMFC/NIP because it does not have imprinted cavities in the
448 polymer structure that only partially hinder the diffusion of methanol/water to the electrode surface. The
449 different assemblies also show differences in OCV values, with PB-DMFC/NIP having the lower OCV
450 value (0.35 V) compared to PB-DMFC/Biosensor (0.41 V) and the unmodified PB-DMFC (0.43 V).
451 Therefore, the time for stable and complete activation is longer for the PB-DMFC/NIP assembly than for
452 PB-DMFC/Biosensor and the unmodified PB-DMFC. The PB-DMFC/NIP could not reach the same
453 potential values due to the barrier effect of the PEDOT/PPy polymer.

454 In the EIS analysis (Figure 4 C), the same PB-DMFC was analysed before/after the polymerization
455 protocol and after calibration. The equivalent electric circuits of these samples were shown in Figure S7.
456 Analysis of the results shows an increase in ohmic resistance and charge transfer after the
457 electropolymerization procedure. After calibration, the PB-DMFC with the sensing layer (PB-DMFC +
458 MIP) shows an increase in ohmic resistance, which could be related to the presence of the sarcosine
459 binding in the polymer cavities.

460

461 *3.4 Calibrations of the PB-DMFC/Biosensor*

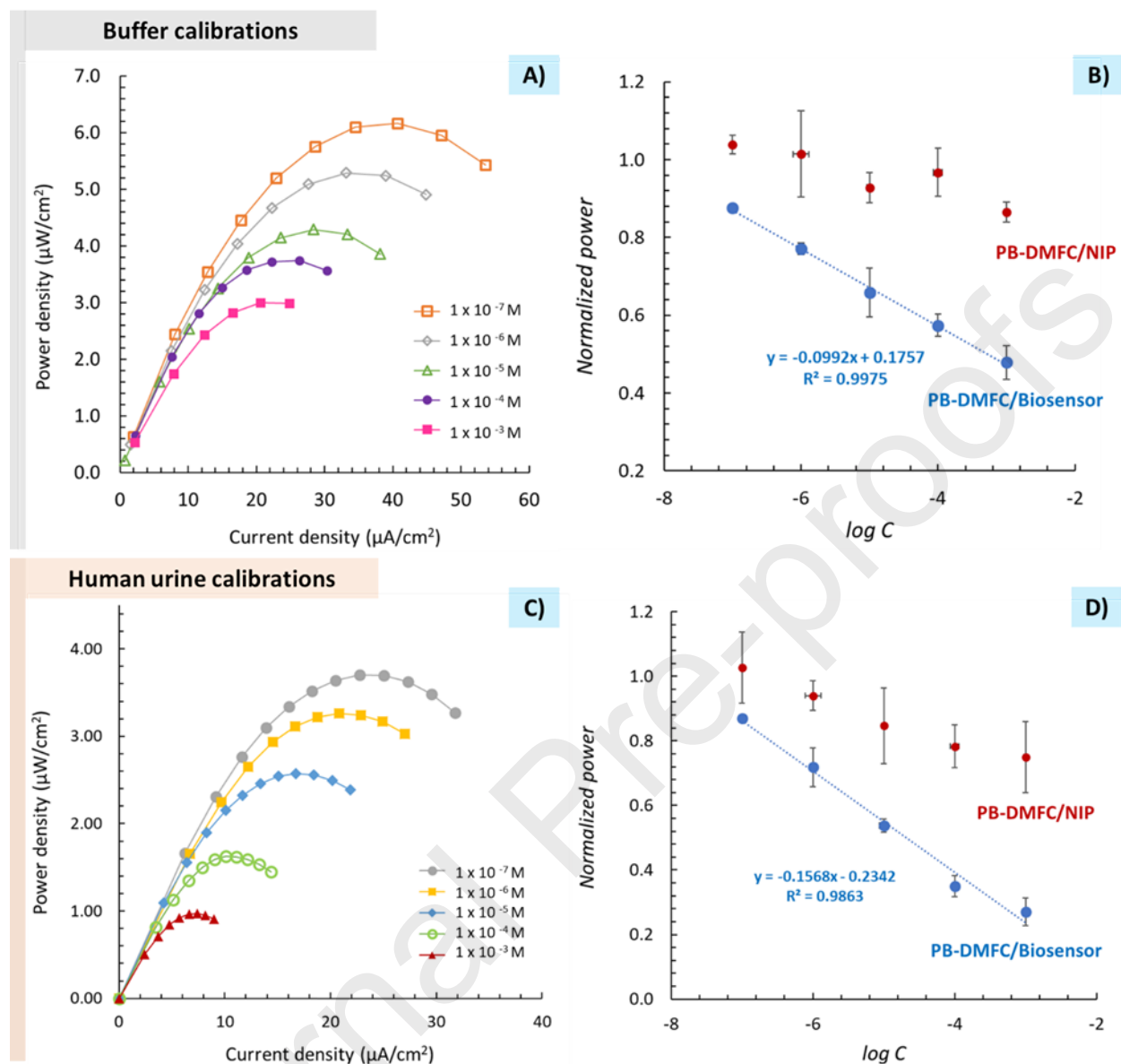
462 The various PB-DMFC/biosensor assemblies were activated by running multiple polarization curves until
463 the systems reached maximum OCV and power levels (the number of polarization curves required for full
464 activation depends on PB-DMFC and can range from 5-10 consecutive trials). After running a polarization
465 curve, the PB-DMFC/biosensor was washed with water, dried with N_2 , and 100 μL of a 0.5 M methanol
466 solution was added. This procedure was repeated continuously throughout the calibration experiment.
467 Prior to calibration, stabilization was performed in the same background medium used to prepare the

468 sarcosine standards by incubating the sensor surface sequentially with the same volume used to incubate
469 the standards (200 μL). This procedure was repeated until stable electrical performance was achieved for
470 both media. Two background media were used to prepare the sarcosine standards: MES Buffer and diluted
471 healthy human urine. This stabilization procedure was essential to ensure that the measured electrical
472 signal was due to the sarcosine interaction and not to the medium in which the standard solution was
473 prepared. In the case of the medium containing healthy human urine, a dilution factor (10 \times and 100 \times) was
474 previously investigated for its effects on signal stability and final performance of the PB-DMFCs
475 assemblies. An example of the stabilization of the PB-DMFC /biosensor assemblies with MES buffer and
476 human urine is shown in [Figure S8](#) in the form of power curves, which show that the successive MES
477 incubations cause little disturbance to the signal compared to the urine incubations ([Figure S8-B-C](#)).
478 Therefore, to obtain a smaller effect on the initial current of the PB-DMFC/biosensor, a 100-fold dilution
479 was chosen for the urine calibrations.

480 After stabilizing the electrical signal of the PB-DMFC/biosensor in the appropriate media,
481 successively increasing concentrations of sarcosine standard solutions in the range of [$1.0 \times 10^{-7} \text{ M} - 1.0$
482 $\times 10^{-3} \text{ M}$] were incubated directly on the surface of the anode sensor, and the polarization curve was
483 followed after incubation of each concentration (from the OCV potential to the predefined final potential
484 of 0.1 V). It is important to highlight that the initial OCV potential of the polarization curve is not the
485 same after each sarcosine standard incubation but decreases over the course of the calibration experiment
486 as the sensor loses the ability to return to initial values when sarcosine is bound in the polymer cavities.
487 The time required to reach a stable OCV potential must be determined at the beginning of the experiment
488 and maintained until the end of the calibration (depending on PB-DMFC, $t=100 \text{ s}$ is sufficient to reach a
489 stable OCV value). The response of a methanol fuel cell biosensor is determined by the oxidation of
490 methanol at the active sites of the Pt catalyst. The kinetics of this reaction is time-dependent and is

491 favoured by the fact that methanol is a small molecule that can easily penetrate through the polymer,
492 depending on the contact time. The major advantage of this system over previously published systems
493 [39,40] is that the methanol solution can be completely removed from the anode sensor region, ensuring
494 that the system is in a similar "true steady state" for all measurements. Each sarcosine standard solution
495 was left on the anode surface for 20 minutes and covered with a square glass to prevent evaporation and
496 ensure efficient distribution of the sample over the entire sensor area. After this time, the PB-
497 DMFC/biosensor was washed with ultrapure water, dried with nitrogen, and 100 μL of a 0.5 M MeOH
498 solution was distributed on the anode side, followed by an electrochemical measurement (OCV
499 stabilization + sampled DC voltammetry technique). This procedure was performed in parallel with a PB-
500 DMFC/NIP to monitor the non-specific interactions of sarcosine in the non-imprinted polymer.

501 Several calibrations were performed to evaluate the standard analytical response of this hybrid paper
502 biosensor. A typical plot of the performance curves obtained during a calibration is shown in [Figure 5A](#)
503 for buffer media, with the average calibration curves in [Figure 5B](#), for PB-DMFC/biosensor compared to
504 the control (PB-DMFC/NIP). [Figure 5C](#) shows a typical calibration obtained in diluted healthy human
505 urine, with the corresponding average calibration curves in [Figure 5D](#). The calibration curves correspond
506 to the normalized maximum peak power calculated for each standard ($\text{power}_{\text{standard}}/\text{power}_{\text{blank}}$).



507

508 **Figure 5.** Power-current density curves obtained during calibration after incubation of sarcosine standards
 509 of increasing concentrations prepared in buffer (A), with the respective calibration curve compared with
 510 a control experiment (NIP) in the range 1.0×10^{-7} - 1.0×10^{-3} mol/L (B); Power-current density curves
 511 obtained during calibration with sarcosine standard solutions prepared in healthy human urine in the same
 512 concentration range used in buffer (C), with the respective calibration curve compared with the NIP
 513 sample (D). All calibration curves were traced using the average of the maximum power density obtained
 514 at each sarcosine concentration.

515

516

517 Analysis of the calibration results shows that the average power density decreases with successive
518 concentrations of the sarcosine standards for both media studied, confirming that it is possible to transform
519 the PB-DMFC activity into a PB-DMFC/biosensor with an operating mode dependent on the sarcosine
520 concentration.

521 For calibrations performed in MES buffer media (Figure 5A), the final PB-DMFC /biosensor output power
522 decreases by ~50% compared to the initial value after blank (background stabilisation) experiments
523 against the maximum sarcosine concentration, with a squared correlation coefficient of ~0.997. This
524 variation was generally consistent between different calibrations performed in buffer when the PB-
525 DMFCs assemblies have similar initial power values. The limit of detection (LoD) was 6.6×10^{-8} M
526 calculated using the equation $LoD = (y_{blank} - 3SD_{blank}) / Slope$. Comparing the PB-DMFC/biosensor with the
527 non-imprinted, PB-DMFC/NIP, a random response can be observed (Figure 5B), indicating minor
528 nonspecific interactions of sarcosine molecules.

529 In the calibrations with human urine (Figure 5C), the final PB-DMFC/biosensor output decreases by ~75%
530 (compared with the initial value after stabilization of the blank) toward the maximum concentration of
531 sarcosine with a squared correlation coefficient of ~0.986. These results demonstrate the good
532 performance of this paper-based biosensor, which can maintain its sensitivity in more complex media such
533 as human urine. Indeed, the results obtained in human urine are more meaningful in terms of impact on
534 fuel cell performance, since the behavior of the PB-DMFC depends entirely on the sarcosine
535 concentration, with a higher impact on the potential, current density, and performance. This behavior
536 highlights that the developed PB-DMFC/biosensor is suitable to target the sarcosine molecule in real
537 samples and can be used in a wide range of concentrations. Considering the non-specific interactions,
538 some differences were observed in the performance curves obtained after the incubation of sarcosine in

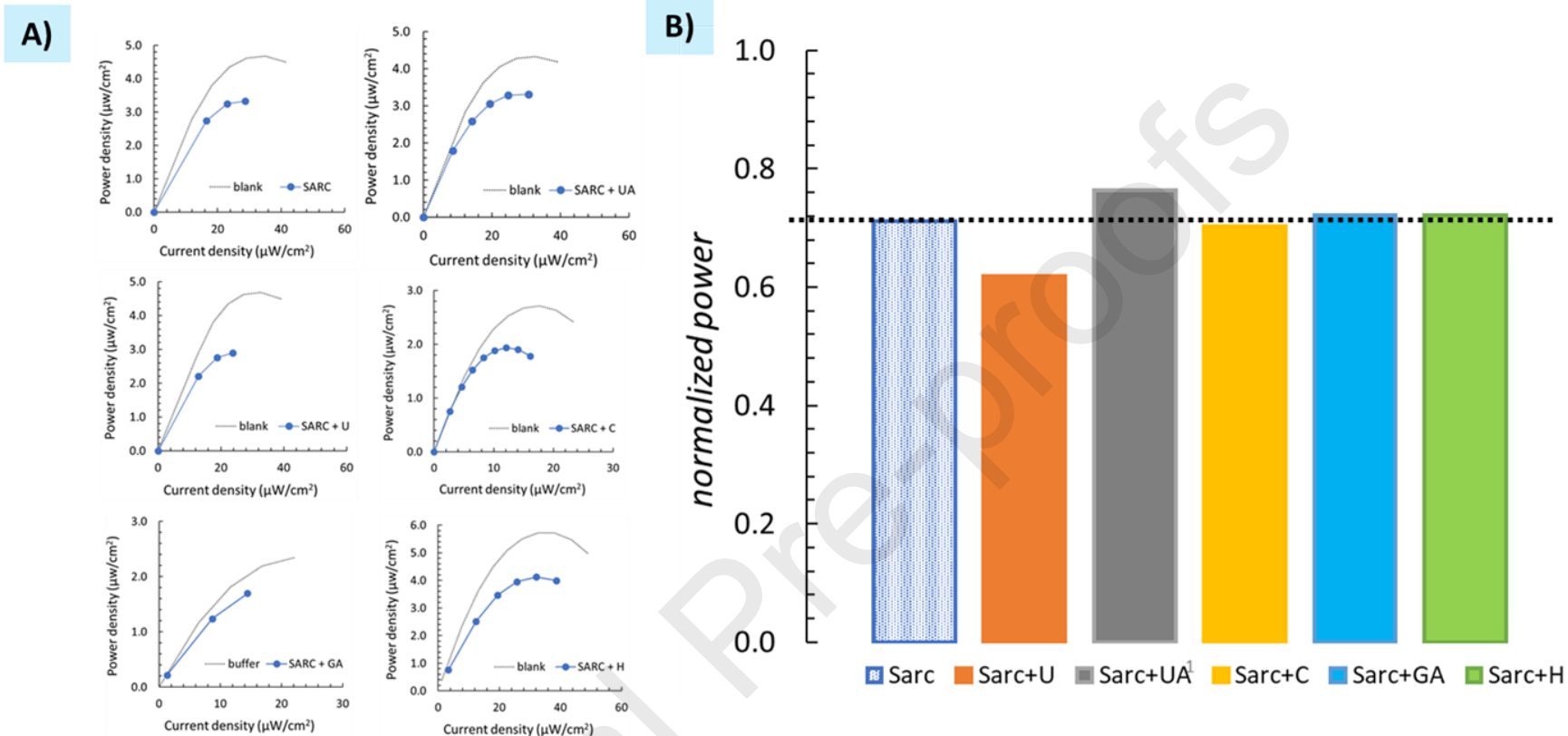
539 the non-imprinted anode (PB-DMFC/NIP) in this medium. However, the response can be considered
540 negligible when compared to the response obtained for the PB-DMFC/biosensor.

541 Thus, this self-powered paper strip PB-DMFC /biosensor can be used for screening and monitoring
542 sarcosine biomarkers without being limited to standard analytical laboratory methods. Common sarcosine
543 oxidase assays can achieve a LoD of 1.18×10^{-6} mol/L with a linear range of $2.05\text{--}125.65 \times 10^{-6}$ mol/L.
544 It is generally accepted that the diagnosis of prostate cancer is associated with elevated levels of sarcosine
545 in body fluids (even in early stages of the disease) [45]. Considering these findings, this autonomous paper
546 platform may be a useful tool to detect abnormal sarcosine levels that may be associated with a prostate
547 cancer diagnosis.

548

549 *3.5 Selectivity studies*

550 To evaluate and complete the selectivity of the designed PB-DMFC/biosensor, selectivity assays were
551 performed in buffer solutions against some common interfering compounds [urea (U), uric acid (UA),
552 creatinine (C), glutamic acid, and histidine (H)]. The assays were performed with different PB-DMFCs
553 units, incubating a sarcosine standard solution (1.0×10^{-5} M) in a PB-DMFC/biosensor. In parallel, the
554 same procedure was repeated with different PB-DMFC/biosensor units by incubating the same
555 concentration of sarcosine with the respective interfering substance. Both PB-DMFC/biosensors were
556 analysed by following their respective polarisation curves. An example of one set of selectivity assays is
557 shown in [Figure 6A](#) with the corresponding interference analysis in [Figure 6B](#).



558

559 **Figure 6.** Selectivity assays in buffer using independent PB-DMFCs after incubation of a sarcosine standard solution (1.0×10^{-5} M) and
 560 sarcosine spiked with interfering compounds [urea (U), uric acid (UA), creatinine (C), glutamic acid and histidine (H)], recording of the
 561 respective power curves (A) and the respective interference analysis in normalized values (B)

562 The data presented in [Figure 6A](#) show that the different PB-DMFCs prepared in the same batch for
563 performing the selectivity assays exhibit a consistent response to the detection of sarcosine, with little
564 signal variation in the presence of interfering factors. These data confirm the high preference of this sensor
565 for sarcosine with signal changes of 1-10%, in both positive and negative directions ([Figure 6B](#)). Urea
566 and uric acid are the interfering factors that cause the largest deviations from the sarcosine signal (10%),
567 while the other interfering factors cause almost no signal change (~1%). The concentrations of all tested
568 interfering factors are compatible with the average values found in real human urine samples, which can
569 support the exceptional performance of this hybrid autonomous fuel cell paper strip.

570

571

572 **4. Conclusions**

573 The developed PB-DMFC/biosensor prototype showed promising results as a self-powered sensing
574 platform for the detection of sarcosine in a hybrid approach combining the potential of a paper methanol
575 fuel cell as an energy source with a MIP sensing element. The improvement in the response of the PB-
576 DMFC/biosensor in real samples (human urine) confirms the high selectivity of the response of this array,
577 which is also confirmed by the different selectivity assays performed.

578 Overall, the presented PB-DMFC/biosensor can be considered as a promising and suitable instrument for
579 point-of-care applications, capable of analysing sarcosine in a wide concentration range, even in complex
580 real samples. The developed PB-DMFC/biosensor opens the doors to a novel strategy in the development
581 of autonomous electrical biosensors by combining two powerful technologies (fuel cells and MIPs).
582 Further improvements of the current prototype in terms of materials used (catalysts, carbon support,
583 electrolyte, impermeabilization), fabrication process, and even different fuels can be explored, opening

584 new opportunities for the expansion of self-powered electrochemical instruments as powerful tools in
585 health diagnostics/monitoring.

586

587 **Acknowledgements**

588 The authors acknowledge the financial support of EU-Horizon 2020 (Symbiotic, FET-Open, GA665046)
589 and LPTC (Grant references: SFRH/BD/122954/2016; COVID/BD/151738/2021) acknowledge
590 Fundação para a Ciência e Tecnologia for financial support. This work was also financially supported by
591 LA/P/0045/2020 (ALiCE), UIDB/00532/2020 and UIDP/00532/2020 (CEFT), funded by national funds
592 through FCT/MCTES (PIDDAC).

593 **5. References**

594

- 595 [1] A.M. López-Marzo, A. Merkoçi, Paper-based sensors and assays: A success of the engineering design and
596 the convergence of knowledge areas, *Lab Chip*. 16 (2016) 3150–3176. <https://doi.org/10.1039/c6lc00737f>.
- 597 [2] S. Marquez, E. Morales-Narváez, Nanoplasmonics in paper-based analytical devices, *Front. Bioeng.*
598 *Biotechnol.* 7 (2019) 1–10. <https://doi.org/10.3389/fbioe.2019.00069>.
- 599 [3] M. Gutiérrez-capitán, A. Baldi, C. Fernández-sánchez, Electrochemical paper-based biosensor devices for
600 rapid detection of biomarkers, *Sensors (Switzerland)*. 20 (2020) 1–15. <https://doi.org/10.3390/s20040967>.
- 601 [4] A.T. Singh, D. Lantigua, A. Meka, S. Taing, M. Pandher, G. Camci-Unal, Paper-based sensors: Emerging
602 themes and applications, *Sensors (Switzerland)*. 18 (2018) 1–22. <https://doi.org/10.3390/s18092838>.
- 603 [5] D. Zhao, Y. Zhu, W. Cheng, W. Chen, Y. Wu, H. Yu, Cellulose-Based Flexible Functional Materials for
604 Emerging Intelligent Electronics, *Adv. Mater.* 33 (2021). <https://doi.org/10.1002/adma.202000619>.
- 605 [6] Y. Zhang, L. Zhang, K. Cui, S. Ge, X. Cheng, M. Yan, J. Yu, H. Liu, Flexible electronics based on
606 micro/nanostructured paper, *Adv. Mater.* 30 (2018). <https://doi.org/10.1002/adma.201801588>.
- 607 [7] Z. Nie, F. Deiss, X. Liu, O. Akbulut, G.M. Whitesides, Integration of paper-based microfluidic devices with
608 commercial electrochemical readers, *Lab Chip*. 10 (2010) 3163–3169. <https://doi.org/10.1039/c0lc00237b>.
- 609 [8] M.M. Gong, D. Sinton, Turning the Page: Advancing Paper-Based Microfluidics for Broad Diagnostic
610 Application, *Chem. Rev.* 117 (2017) 8447–8480. <https://doi.org/10.1021/acs.chemrev.7b00024>.
- 611 [9] T. Ozer, C. McMahon, C.S. Henry, Advances in Paper-Based Analytical Devices, *Annu. Rev. Anal. Chem.*
612 13 (2020) 85–109. <https://doi.org/10.1146/annurev-anchem-061318-114845>.
- 613 [10] J. Mettakoonpitak, K. Boehle, S. Nantaphol, P. Teengam, J.A. Adkins, M. Srisa-Art, C.S. Henry,
614 Electrochemistry on Paper-based Analytical Devices: A Review, *Electroanalysis*. 28 (2016) 1420–1436.
615 <https://doi.org/10.1002/elan.201501143>.
- 616 [11] Y. Xia, J. Si, Z. Li, Fabrication techniques for microfluidic paper-based analytical devices and their
617 applications for biological testing: A review, *Biosens. Bioelectron.* 77 (2016) 774–789.
618 <https://doi.org/10.1016/j.bios.2015.10.032>.
- 619 [12] E. Noviana, C.S. Henry, Simultaneous electrochemical detection in paper-based analytical devices, *Curr.*
620 *Opin. Electrochem.* 23 (2020) 1–6. <https://doi.org/10.1016/j.coelec.2020.02.013>.

- 621 [13] T. Akyazi, L. Basabe-Desmonts, F. Benito-Lopez, Review on microfluidic paper-based analytical devices
622 towards commercialisation, *Anal. Chim. Acta.* 1001 (2018) 1–17. <https://doi.org/10.1016/j.aca.2017.11.010>.
- 623 [14] L.L. Shen, G.R. Zhang, T. Venter, M. Biesalski, B.J.M. Etzold, Towards best practices for improving paper-
624 based microfluidic fuel cells, *Electrochim. Acta.* 298 (2019) 389–399.
625 <https://doi.org/10.1016/j.electacta.2018.12.077>.
- 626 [15] S.A. Mousavi Shaegh, N.T. Nguyen, S.H. Chan, Air-breathing microfluidic fuel cell with fuel reservoir, *J.*
627 *Power Sources.* 209 (2012) 312–317. <https://doi.org/10.1016/j.jpowsour.2012.02.115>.
- 628 [16] S. Chandra, S. Lal, V.M. Janardhanan, K.C. Sahu, M. Deepa, Ethanol based fuel cell on paper support, *J.*
629 *Power Sources.* 396 (2018) 725–733. <https://doi.org/10.1016/j.jpowsour.2018.06.068>.
- 630 [17] Y. Wang, H.Y.H. Kwok, Y. Zhang, W. Pan, H. Zhang, X. Lu, D.Y.C. Leung, A flexible paper-based
631 hydrogen fuel cell for small power applications, *Int. J. Hydrogen Energy.* 44 (2019) 29680–29691.
632 <https://doi.org/10.1016/j.ijhydene.2019.04.066>.
- 633 [18] I.D.M. De Barcelona, I. Csic, DISPOSABLE HYDROGEN FUEL CELLS FOR POWERING NEXT-
634 GENERATION University of Washington , Department of Bioengineering , Seattle , WA , USA Instituto
635 de Catálisis y Petroleoquímica , ICP (CSIC), Madrid , SPAIN, (2015) 66–69.
- 636 [19] J.P. Esquivel, F.J. Del Campo, J.L. Gómez De La Fuente, S. Rojas, N. Sabaté, Microfluidic fuel cells on
637 paper: Meeting the power needs of next generation lateral flow devices, *Energy Environ. Sci.* 7 (2014) 1744–
638 1749. <https://doi.org/10.1039/c3ee44044c>.
- 639 [20] R.K. Arun, S. Halder, N. Chanda, S. Chakraborty, A paper based self-pumping and self-breathing fuel cell
640 using pencil stroked graphite electrodes, *Lab Chip.* 14 (2014) 1661–1664.
641 <https://doi.org/10.1039/c4lc00029c>.
- 642 [21] S. Lal, V.M. Janardhanan, M. Deepa, A. Sagar, K.C. Sahu, Low Cost Environmentally Benign Porous Paper
643 Based Fuel Cells for Micro-Nano Systems, *J. Electrochem. Soc.* 162 (2015) F1402–F1407.
644 <https://doi.org/10.1149/2.0251514jes>.
- 645 [22] F. Achmad, S.K. Kamarudin, W.R.W. Daud, E.H. Majlan, Passive direct methanol fuel cells for portable
646 electronic devices, *Appl. Energy.* 88 (2011) 1681–1689. <https://doi.org/10.1016/j.apenergy.2010.11.012>.
- 647 [23] T. Wilberforce, A. Alaswad, A. Palumbo, M. Dassisti, A.G. Olabi, Advances in stationary and portable fuel
648 cell applications, *Int. J. Hydrogen Energy.* 41 (2016) 16509–16522.
649 <https://doi.org/10.1016/j.ijhydene.2016.02.057>.

- 650 [24] E.J. Ryan, E.M. Creagh, Emerging methods in colorectal cancer screening, *Br. J. Surg.* 105 (2018) e16–e18.
651 <https://doi.org/10.1002/bjs.10650>.
- 652 [25] M. Piert, X. Shao, D. Raffel, M.S. Davenport, J. Montgomery, L.P. Kunju, B.G. Hockley, J. SidDiqui, P.J.H.
653 Scott, A.M. Chinnaiyan, T. RajenDiran, Preclinical evaluation of ¹¹C-sarcosine as a substrate of proton-
654 coupled amino acid transporters and first human application in prostate cancer, *J. Nucl. Med.* 58 (2017)
655 1216–1223. <https://doi.org/10.2967/jnumed.116.173179>.
- 656 [26] G. Ploussard, A. De La Taille, Urine biomarkers in prostate cancer, *Nat. Rev. Urol.* 7 (2010) 101–109.
657 <https://doi.org/10.1038/nrurol.2009.261>.
- 658 [27] C.S. Pundir, R. Deswal, P. Kumar, Quantitative analysis of sarcosine with special emphasis on biosensors:
659 a review, *Biomarkers.* 24 (2019) 415–422. <https://doi.org/10.1080/1354750X.2019.1615124>.
- 660 [28] A.P. Khan, T.M. Rajendiran, B. Ateeq, I.A. Asangani, J.N. Athanikar, A.K. Yocum, R. Mehra, J. Siddiqui,
661 G. Palapattu, J.T. Wei, G. Michailidis, A. Sreekumar, A.M. Chinnaiyan, The role of sarcosine metabolism
662 in prostate cancer progression, *Neoplasia (United States).* 15 (2013) 491–501.
663 <https://doi.org/10.1593/neo.13314>.
- 664 [29] A. Roy, Y.P. Chen, J.T. Qiu, S. Maikap, Sarcosine Prostate Cancer Biomarker Detection by Controlling
665 Oxygen in NiOxMembrane on Vertical Silicon Nanowires in Electrolyte-Insulator-Nanowire Structure,
666 *Anal. Chem.* 92 (2020) 8064–8071. <https://doi.org/10.1021/acs.analchem.9b04745>.
- 667 [30] J.N. Tiwari, R.N. Tiwari, G. Singh, K.S. Kim, Recent progress in the development of anode and cathode
668 catalysts for direct methanol fuel cells, *Nano Energy.* 2 (2013) 553–578.
669 <https://doi.org/10.1016/j.nanoen.2013.06.009>.
- 670 [31] M.S. Alias, S.K. Kamarudin, A.M. Zainoodin, M.S. Masdar, Structural mechanism investigation on
671 methanol crossover and stability of a passive direct methanol fuel cell performance via modified micro-
672 porous layer, *Int. J. Energy Res.* 45 (2021) 12928–12943. <https://doi.org/10.1002/er.6624>.
- 673 [32] T.S. Zhao, R. Chen, W.W. Yang, C. Xu, Small direct methanol fuel cells with passive supply of reactants,
674 *J. Power Sources.* 191 (2009) 185–202. <https://doi.org/10.1016/j.jpowsour.2009.02.033>.
- 675 [33] R. Chen, T.S. Zhao, A novel electrode architecture for passive direct methanol fuel cells, *Electrochem.*
676 *Commun.* 9 (2007) 718–724. <https://doi.org/10.1016/j.elecom.2006.11.004>.
- 677 [34] Y. Zhang, D.P. Wilkinson, F. Taghipour, Performance Analysis of an Air-Breathing Micro-Direct Methanol
678 Fuel Cell with an Extended Anode Region, *Fuel Cells.* 20 (2020) 634–642.
679 <https://doi.org/10.1002/fuce.201900165>.

- 680 [35] Z. Long, L. Gong, Y. Sun, Y. Li, P. Xu, X. Zhang, J. Ge, C. Liu, S. Ma, Z. Jin, In-situ precise electrocatalytic
681 behaviors of Pt/C and PtRu/C for methanol oxidation of DMFCs via the designed micro-MEA, *Int. J.*
682 *Hydrogen Energy*. 43 (2018) 12413–12419. <https://doi.org/10.1016/j.ijhydene.2018.05.024>.
- 683 [36] L. Bokobza, J.L. Bruneel, M. Couzi, Raman spectroscopic investigation of carbon-based materials and their
684 composites. Comparison between carbon nanotubes and carbon black, *Chem. Phys. Lett.* 590 (2013) 153–
685 159. <https://doi.org/10.1016/j.cplett.2013.10.071>.
- 686 [37] W.W. Chiu, J. Travaç, R.P. Cooney, G.A. Bowmaker, Spectroscopic and conductivity studies of doping in
687 chemically synthesized poly(3,4-ethylenedioxythiophene), *Synth. Met.* 155 (2005) 80–88.
688 <https://doi.org/10.1016/j.synthmet.2005.06.012>.
- 689 [38] M.S. Dresselhaus, A. Jorio, R. Saito, Characterizing graphene, graphite, and carbon nanotubes by Raman
690 spectroscopy, *Annu. Rev. Condens. Matter Phys.* 1 (2010) 89–108. <https://doi.org/10.1146/annurev-conmatphys-070909-103919>.
- 691
- 692 [39] L.P.T. Carneiro, A.M.F.R. Pinto, A. Mendes, M. Goreti, An all-in-one approach for self-powered sensing:
693 A methanol fuel cell modified with a molecularly imprinted polymer for cancer biomarker detection, *J.*
694 *Electroanal. Chem.* 906 (2022) 116009. <https://doi.org/10.1016/j.jelechem.2022.116009>.
- 695 [40] L.P.T. Carneiro, N.S. Ferreira, A.P.M. Tavares, A.M.F.R. Pinto, A. Mendes, M.G.F. Sales, A passive direct
696 methanol fuel cell as transducer of an electrochemical sensor, applied to the detection of carcinoembryonic
697 antigen, *Biosens. Bioelectron.* 175 (2021) 1–9. <https://doi.org/10.1016/j.bios.2020.112877>.
- 698 [41] M.M. Ghosh S, Das S, Conducting Polymer-Based Nanohybrids for Fuel Cell Application, *Polym.* 15 (2020)
699 1–19. doi: 10.3390/polym12122993. PMID: 33333881; PMCID: PMC7765313.
- 700 [42] K.K. Tintula, S. Pitchumani, P. Sridhar, A.K. Shukla, A solid-polymer-electrolyte direct methanol fuel cell
701 (DMFC) with Pt-Ru nanoparticles supported onto poly(3,4-ethylenedioxythiophene) and polystyrene
702 sulphonic acid polymer composite as anode, *J. Chem. Sci.* 122 (2010) 381–389.
703 <https://doi.org/10.1007/s12039-010-0043-6>.
- 704 [43] C.F. Hsu, L. Zhang, H. Peng, J. Travas-Sejdic, P.A. Kilmartin, Free radical scavenging properties of
705 polypyrrole and poly(3,4-ethylenedioxythiophene), *Curr. Appl. Phys.* 8 (2008) 316–319.
706 <https://doi.org/10.1016/j.cap.2007.10.049>.
- 707 [44] J.M. Lin, Y.L. Su, W.T. Chang, W.Y. Su, S.H. Cheng, Strong adsorption characteristics of a novel
708 overoxidized poly(3,4-ethylenedioxythiophene) film and application for dopamine sensing, *Electrochim.*
709 *Acta.* 149 (2014) 65–75. <https://doi.org/10.1016/j.electacta.2014.10.030>.

710 [45] M. Wang, L. Zou, J. Liang, X. Wang, D. Zhang, Y. Fang, J. Zhang, F. Xiao, M. Liu, The urinary
 711 sarcosine/creatinine ratio is a potential diagnostic and prognostic marker in prostate cancer, Med. Sci. Monit.
 712 24 (2018) 3034–3041. <https://doi.org/10.12659/MSM.909949>.

713

714 **Development of an innovative flexible paper-based methanol fuel cell**
 715 **(PB-DMFC) sensing platform –application to sarcosine detection**

716 *Liliana P. T. Carneiro*^{*1,2,3,4}, *Alexandra M. F. R. Pinto*⁴, *M. Goreti F. Sales*^{**1,2}

717 ¹BioMark@UC, Department of Chemical Engineering, Faculty of Sciences and Technology,

718 Coimbra University, Portugal

719 ²BioMark@ISEP, School of Engineering, Polytechnic Institute of Porto, Portugal

720 ³CEB, Centre of Biological Engineering, Minho University, Portugal

721 ⁴CEFT, Department of Chemical Engineering, Faculty of Engineering, University of Porto, Portugal

722

723

724 **Declaration of interests**

725 The authors declare that they have no known competing financial interests or personal relationships
 726 that could have appeared to influence the work reported in this paper.

727 The authors declare the following financial interests/personal relationships, which may be considered
 728 as potential competing interests:

729

730

731 **The authors,**

732

733 Liliana Carneiro

734 Alexandra Pinto

735 Goreti Sales

736 1 2 9 0

737 UNIVERSIDADE DE
 COIMBRA



738

739

740

741 Porto, 30th of May of 2021

742

743

744 **Highlights**

745 *Development of an innovative flexible paper-based methanol fuel cell (PB-DMFC) sensing platform –*
746 *application to sarcosine detection*

- 747 ➤ Novel hand-made methanol fuel cell designed on a paper substrate
- 748 ➤ Cathode and anode designed in both sides of the paper substrate
- 749 ➤ Anode modified with a molecularly imprinted polymer for sarcosine
- 750 ➤ Fuel cell operation dependent upon sarcosine concentration
- 751 ➤ Sarcosine as a cancer biomarker that needs to be monitored

752